HHS Public Access

Author manuscript

FASEB J. Author manuscript; available in PMC 2024 September 01.

Published in final edited form as:

FASEB J. 2023 September ; 37(9): e23156. doi:10.1096/fj.202300349R.

Muscle p62 stimulates the expression of antioxidant proteins alleviating cancer cachexia

Mami Yamada[1], **Eiji Warabi**[2], **Hisashi Oishi**[3], **Vitor A. Lira**[4], **Mitsuharu Okutsu**[1]

[1]Graduate School of Science, Nagoya City University, Nagoya, Japan.

[2]Faculty of Medicine, University of Tsukuba, Tsukuba, Japan.

[3]Department of Comparative and Experimental Medicine, Nagoya City University Graduate School of Medical Sciences, Nagoya, Japan.

[4]Department of Health and Human Physiology, Obesity Research and Education Initiative, F.O.E. Diabetes Research Center, Abboud Cardiovascular Research Center, Pappajohn Biomedical Institute, The University of Iowa, IA, USA.

Abstract

Oxidative stress plays an important role in skeletal muscle atrophy during cancer cachexia, and more glycolytic muscles are preferentially affected. Sequestosome1/SQSTM1 (i.e., p62), particularly when phosphorylated at Ser 349 (Ser 351 in mice), competitively binds to the Kelch-like ECH-associated protein 1 (Keap1) activating Nuclear factor erythroid 2-related factor 2 (Nrf2). Nrf2 then stimulates transcription of antioxidant/electrophile responsive elements in target genes. However, a potential role for p62 in the protection of muscle wasting in cachexia remains to be determined. Here, using the well-established cachexia-inducing model of Lewis Lung Carcinoma (LLC) in mice we demonstrate higher expression of antioxidant proteins (i.e., NQO1, HO-1, GSTM1, CuZnSOD, MnSOD, and EcSOD) in the more oxidative and cachexia resistant soleus muscle than in the more glycolytic and cachexia prone extensor digitorum longus muscle. This was accompanied by higher p62 (total and phosphorylated) and nuclear Nrf2 levels in the soleus, which were paralleled by higher expression of proteins known to either phosphorylate or promote p62 phosphorylation (i.e., NBR1, CK1, PKCδ, and TAK1). Muscle-specific p62 gain-of-function (i.e., in p62 mTg mice) activated Nrf2 nuclear translocation and increased the expression of multiple antioxidant proteins (i.e., CuZnSOD, MnSOD, EcSOD, NQO1 and GSTM1) in glycolytic muscles. Interestingly, skeletal muscle Nrf2 haplodeficiency blunted the increases of most of these proteins (i.e., CuZnSOD, EcSOD, and NQO1) suggesting that muscle p62 stimulates antioxidant protein expression also via additional, yet to be determined mechanisms. Of note, p62 gain-of-function mitigated glycolytic muscle wasting in LLC affected

Corresponding author: Mitsuharu Okutsu, Ph.D., Graduate School of Sciences, Nagoya City University, Address: Yamanohata 1, Mizuho-cho, Mizuho-ku, Nagoya, Aichi 467-8501, Japan, TEL: +81-52-872-5837, okutsu@nsc.nagoya-cu.ac.jp.

Author Contributions

M.Y. and M.O. conceived and designed research; M.Y., E.W., H.O., and M.O. performed experiments; M.Y. and M.O. analyzed data; M.Y., V.A.L., and M.O. interpreted results of experiments; M.Y., V.A.L., and M.O. prepared figures and tables; M.Y., V.A.L., and M.O. wrote the manuscript.

Conflict of Interest

All authors have no conflict of interest.

mice. Collectively, our findings identify skeletal muscle p62 as a potential therapeutic target for cancer cachexia.

Graphical Abstract:

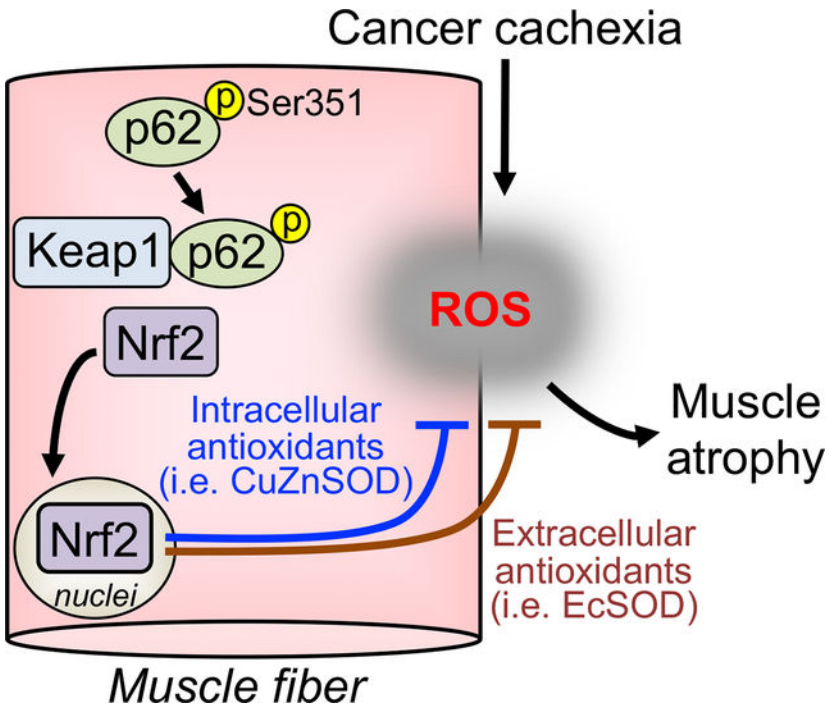

Cancer cachexia increases oxidative stress and induces skeletal muscle atrophy, particularly in glycolytic muscles. Here, using a Lewis Lung Carcinoma-induced cachexia model, we demonstrated that the p62-Nrf2 pathway is more active in oxidative muscles when compared to glycolytic muscles. Mice with enhanced p62 expression in muscle have increased intra- and extracellular antioxidant proteins expression, and this induction were partially inhibited by Nrf2 haplodeficiency. Furthermore, p62 overexpression suppressed oxidative stress and alleviated glycolytic muscle atrophy in cancer cachexia.

Keywords

Skeletal muscle; Muscle atrophy; Oxidative stress; Antioxidants; SQSTM1/p62; Nrf2

Introduction

Cancer cachexia is characterized by a significant reduction in body weight predominantly resulting from severe loss of skeletal muscle. Cachexia occurs in up to 80% of cancer patients and directly contributes to up to 30% of cancer-related deaths (1, 2). Oxidative stress, which is caused by excessive production of reactive oxygen species and/or declined antioxidant defense plays an important role in muscle atrophy during cancer cachexia, particularly in muscle predominantly containing glycolytic fibers (3, 4). However, molecular

mechanisms regulating the expression of antioxidant proteins that may protect against muscle wasting in the context of cancer cachexia remain to be determined.

Although multiple molecular pathways regulate antioxidant protein expression in response to cellular stress, a major signal is mediated by the Kelch-like ECH-associated protein 1 (Keap1)-nuclear factor erythroid 2-related factor 2 (Nrf2) pathway (5, 6). Under non-stressed conditions, Nrf2 nuclear translocation is limited due to its physical interaction with Keap1 in the cytoplasm, which also leads to rapid Nrf2 degradation by the ubiquitin-proteasome system (7, 8). In contrast, different types of cellular stress cause Nrf2 to dissociate from Keap1, translocate to the nucleus, form heterodimers with small musculoaponeurotic fibrosarcoma proteins, and bind to the antioxidant/electrophile responsive element (ARE/EpRE) - a cis-acting element in the promoter region of target genes (9, 10). Nrf2 regulates the expression of a set of cytoprotective antioxidant genes, such as NAD(P)H-quinone oxidoreductase 1 (NQO1), heme oxygenase 1 (HO-1), glutathione S-transferase (GST), and superoxide dismutase (SOD) in skeletal muscle (6, 11, 12), suggesting that Nrf2 activation is important for a robust antioxidant defense system and may be beneficial in cancer cachexia.

Sequestosome1/SQSTM1 (p62) plays an important role in the regulation of Nrf2 activation and antioxidant expression (13). In fact, in hepatocellular carcinoma cells, phosphorylation of p62 at Ser349 (Ser351 in mice) increases its affinity for Keap1, competing away Nrf2 for Keap1 binding, which then leads to Nrf2 nuclear translocation, Nrf2 ARE binding, and stimulation of antioxidant gene transcription (14, 15). However, the following remains to be determined: 1) whether p62 regulates antioxidant protein expression in skeletal muscle; 2) if so, whether Nrf2 activation by p62 is essential for enhancement of antioxidants in skeletal muscle; and 3) whether enhanced p62 expression protects against muscle wasting in cancer cachexia.

Here, using muscle-specific gene deletion and overexpression in mice, we report that p62 gain-of-function leads to higher expression of several antioxidant genes in skeletal muscles largely via Nrf2 activation. We also reveal that increased p62 expression alleviates muscle atrophy in Lewis Lung Carcinoma (LLC)-induced cancer cachexia.

Materials and Methods

Animals

C57BL/6J mice were obtained from Japan SLC (Shizuoka, Japan) and were studied at 8 weeks old. p62 muscle-specific overexpression (p62 mTg) mice were generated with p62 cDNA placed downstream of muscle creatine kinase (MCK) promoter (16–18). From the 8 lines of p62 mTg mice obtained, we selected two lines showing graded expression of p62 and designated them low (line L) and high expression (line H). Mice with muscle-specific p62 overexpression and skeletal muscle-specific Nrf2 haplodeficiency (p62 mTg/Nrf2 skmHET) were generated by crossing line H of p62 mTg mice with a myosin light chain 1 fast promoter (Mlc1f)-Cre/Nrf2$^{f/f}$ (Nrf2 skmKO) mice. Nrf2 skmKO mice were generated by crossing mice bearing a floxed Nrf2 allele (Nrf2$^{f/f}$) with transgenic mice expressing Cre under the control of a Mlc1f (19–22). Mlc1f-Cre mice and Nrf2 floxed mice were

generously provided by Dr. Steven J. Burden (New York University, New York, NY, USA) and Dr. Jinbo Pi (China Medical University, Shenyang, China), respectively. Mlc1f-Cre and MCK activity have been detected in both glycolytic and oxidative muscles (16, 19, 22). p62 mTg and p62 mTg/Nrf2 skmHET mice were studied at 8 wks of age. The results in p62 mTg mice were compared with age-matched wild-type (WT) littermate mice, and results in p62 mTg/Nrf2 skmHET mice were compared with age-matched $Nrf2^{f/+}$, Mlc1f-Cre/$Nrf2^{f/+}$, and p62 mTg/$Nrf2^{f/+}$ mice. The animals were provided access to food and drinking water *ad libitum*. After animals were euthanized, blood, muscles (tonic oxidative soleus, mixed fiber type plantaris, tibialis anterior and gastrocnemius, and phasic glycolytic white vastus lateralis and extensor digitorum longus), and spleen were harvested for analysis. In addition, heart, liver, lung, and kidney were harvested to confirm appropriate gene targeting in all models. All of the experimental procedures were carried out with the approval from the Ethical Committee of Nagoya City University (H26M-71 and H30M-40).

Genotyping

Mouse DNA was isolated following a phenol-chloroform–based DNA extraction protocol and used for PCR with primers for the Mlc1f-Cre allele, the loxP-flanked Nrf2 allele, and MCK-p62 allele (22). Reactions consisted of 1 minute of initial denaturation at 94°C, 35 cycles of denaturation (98°C for 5 seconds), annealing (55°C for 5 seconds), and extension (72°C for 10 seconds), and a final 3min extension at 72°C. PCR products were resolved through electrophoresis on a 2% agarose gel containing AtlasSight DNA Stain (BioAtlas, Tartu, Estonia), followed by image acquisition with an ImageQuant LAS 500 (GE Healthcare, Chicago, IL, USA). Mice with a genotype of MCK^+ was considered p62mTg, and mice with a genotype of MCK^- was considered WT littermates for p62 mTg. Mice with a genotype of Mlc1f-Cre;$Nrf2^{f/f}$ was considered Nrf2 skmKO. Mice with a genotype of MCK; Mlc1f-Cre;$Nrf2^{f/+}$ was considered p62 mTg/Nrf2 skmHET mice. Mouse genotypes were confirmed by western blot or semiquantitative RT-PCR analysis.

LLC cells growth and tumor implantation

Lewis Lung Carcinoma (LLC) cells (JCRB Cell Bank, JCRB1348) were cultured in 175 cm^2 culture flasks in RPMI 1640 containing, 300 μg glutamine, 25 mmol HEPES, 10% fetal bovine serum, 100 IU/ml penicillin, and 100 μg/ml streptomycin (culture medium). These cells were trypsinized, counted, and diluted in culture medium for implantation. LCC cells (1×10^7) suspended in 200 μL of sterile PBS were implanted subcutaneously to the hind flank of mice at 8 weeks of age as previously described (23–25). For sham control, age matched male WT, p62 mTg and WT littermates for p62 mTg were injected with 200 μL of sterile PBS. Mice were harvested 4 weeks after LLC or PBS injection.

Treadmill running test

Mice were acclimated to treadmill running for 3 days (~13.4 m/min, 10 min). On the fourth day, animals were tested on the treadmill starting with a speed of 13.4 m/min and 5% incline. The speed was increased by 2.7m/min every 30 min until reaching a speed of 26.8m/min. A paper towel located at the end of the treadmill was used to encourage the animals to run, and the test was terminated when a mouse stopped responding to continuous tail brushing for 20 s (22).

Grip strength test

A grip strength test was performed at the end of the intervention using a grip strength meter (GPM-101B; Melquest, Toyama, Japan) according to the manufacturer's instructions. Each mouse was tested using 10 trials with 10 second-intervals. The mean value of the 2 highest readings normalized by body weight (excluding tumor weight) was used for statistical analysis (22).

Hematoxylin and Eosin (HE) staining

Tibialis anterior muscles were harvested and frozen in liquid nitrogen-cooled isopentane. Cross sections (8 μm) of the tibialis anterior muscle were stained with eosin Y working solution (Sigma-Aldrich, St. Louis, MO, USA), rinsed with distilled water, and counterstained with Mayer's hematoxylin (Muto Pure Chemicals, Tokyo, Japan). Sections were rinsed again with distilled water, dehydrated in ethanol, and mounted on slides with mounting medium as described above. Images were acquired with a DS-Fi1 digital camera (Nikon, Tokyo, Japan) coupled to a BX43 optical microscope (Olympus, Tokyo, Japan)(22).

Muscle fiber size

Muscle fiber size was assessed by immunofluorescence of myosin heavy chain (MyHC) I, IIa and MyHCIIb, as described previously (26). Fresh frozen tibialis anterior muscle sections (8 μm) were incubated with primary antibodies for MyHCI (BA-F8, RRID:AB_10572253; DSHB, Iowa City, USA), MyHCIIa (SC-71, RRID:AB_2147165; DSHB), and MyHCIIb (BF-F3, RRID:AB_2266724; DSHB) overnight at 4°C, then incubated with fluorescent dye-conjugated secondary antibodies for goat anti-mouse IgG Alexa Fluor 405 (ab175660; Abcam, Cambridge, United Kingdom) and goat anti-mouse IgM Alexa Fluor 488 (ab150121; Abcam) for 1 hour at room temperature. Sections were then mounted with Vectashield mounting medium (Vector Laboratories, Burlingame, CA), and images were captured using an ECLIPS Ti-S fluorescent microscope (Nikon, Tokyo, Japan). Non-stained fibers were analyzed as MyHCIId/x. Muscle fiber-size was determined with ImageJ software through examination of more than 100 fibers/sample.

Western blots

Whole muscles were homogenized on ice in sample lysis buffer containing protease and phosphatase inhibitors using a glass-on-glass homogenizer as previously described (27). Tissue debris were discarded after centrifugation at 12,000 g for 3 minutes. Protein concentrations were determined using the DC protein assay (Bio-Rad, Hercules, CA, USA). Muscle lysates (40 μg) were separated by PAGE and transferred overnight at 4°C to PVDF membranes for Western blotting. Ponceau S stain was used to verify appropriate loading and transfer of proteins to membranes. Immunoblot analysis was performed with the following primary antibodies: Atrogin-1/MAFbx (sc166806, RRID:AB_2246982; Santa Cruz Biotechnology, Santa Cruz, CA, USA), MuRF1 (SC398608, RRID:AB_2819249; Santa Cruz Biotechnology), CuZnSOD (ab16831, RRID:AB_302535; Abcam), MnSOD (ab13534, RRID:AB_2191667; Abcam), EcSOD (AF4817, RRID:AB_2270682; R&D Systems, Minneapolis, MN, USA), NQO1 (NB100–1005, RRID:AB_10002672; Novus Biologicals, Centennial, CO, USA), HO-1 (ADI-

OSA-111, RRID:AB_10618556; Enzo Life Science, Farmingdale, NY, USA), GSTM1 (sc517262, RRID:N/A; Santa Cruz Biotechnology), Nrf2 (SC722, RRID:AB_2108502; Santa Cruz Biotechnology and16396–1-AP, RRID:AB_2782956; Proteintech, Rosemont, IL, USA), Keap1 (10503–2-AP, RRID:AB_2132625; Proteintech), phosphorylated-p62 Ser351 (PM074, RRID:N/A; MBL Life Science, Nagoya, Japan), phosphorylated-p62 Ser403 (D343–3, RRID:N/A; MBL Life Science), p62 (p0067, RRID:AB_1841064; MilliporeSigma, Burlington, MA, USA), NBR1 (sc130380, RRID:AB_2149402; Santa Cruz Biotechnology), CK1 (2655, RRID:AB_2283593; Cell Signaling Technology, Danvers, MA, USA), PKCδ (2058, RRID:AB_10694655; Cell Signaling Technology), TAK1 (4505, RRID:AB_490858; Cell Signaling Technology), MyHCI (BA-F8, RRID:AB_10572253; DSHB), MyHCIIa (SC-71, RRID:AB_2147165; DSHB), MyHCIIb (BF-F3, RRID:AB_2266724; DSHB), PGC-1α (AB3242, RRID:AB_2268462; Millipore, Darmstadt, Germany), COX IV (4844, RRID:AB_2085427; Cell Signaling Technology), Cytochrome C (4272, RRID:AB_2090454; Cell signaling Technology), LC3 (4108, RRID:AB_2137703; Cell signaling Technology), Atg6/Beclin1 (3738, RRID:AB_490837; Cell Signaling Technology), Atg7 (2631, RRID:AB_2227783; Cell Signaling Technology), Lamin B1 (9087, RRID:AB_10896336; Cell Signaling Technology), and αβ tubulin (2148, RRID: AB_2288042; Cell Signaling Technology). Immunoblot images were captured by ImageQuant LAS 500 (GE Healthcare, Chicago, IL, USA) and quantified with ImageJ software (National Institutes of Health, Bethesda, MD, USA).

Oxidative stress analysis

To assess oxidative stress in skeletal muscle, whole soleus and white vastus lateralis muscles were homogenized on ice in sample lysis buffer containing 50 mM Tris-HCl (pH 6.8), 1% sodium dodecyl sulfate (SDS), 10% glycerol, 20 mM dithiothreitol, and 0.01% bromophenol blue, supplemented with protease inhibitor. Cell debris were discarded after centrifugation at 12,000 g for 3 minutes. and subsequently assayed for protein concentration using the DC protein assay (Bio-Rad). Muscle lysates (40 μg) were separated by PAGE and transferred overnight at 4°C to PVDF membranes for Western blotting. Malondialdehyde (MDA) (MMD-030n, RRID:AB_605072; JaICA, Shizuoka, Japan) was normalized to Ponceau S as described for Western blots.

Isolation of nuclear and cytoplasmic fractions

Nuclear and cytoplasmic fractions were isolated from the red (oxidative) portion of the gastrocnemius, the white (glycolytic) portion of the gastrocnemius, and the predominant glycolytic extensor digitorum longus muscles to establish Nrf2 nuclear translocation (22). Fractionations were performed using NE-PER™ Nuclear and Cytoplasmic Extraction Reagents (Thermo Scientific). Essentially, gastrocnemius muscles were carefully separated into red and white portions. Isolated red and white portion of gastrocnemius and whole extensor digitorum longus muscle were gently glass-on-glass homogenized in CER I buffer on ice. Homogenized samples were transferred to microtubes and incubated for 10 minutes on ice before CER II buffer was added. Samples were then vortexed vigorously for 5 seconds and centrifuged at 16,000 g for 5 minutes at 4°C. Supernatants containing the cytoplasmic fraction were transferred to prechilled microtubes. NER buffer was added to the nuclear pellets and incubated for 40 minutes on ice, after which samples were centrifuged

at 16,000 g for 10 minutes at 4°C. The resulting supernatant was analyzed as the nuclear fraction.

Immunoprecipitation

A portion of the white (glycolytic) portion of gastrocnemius was homogenized on ice in sample lysis buffer containing 20 mM Tris-HCl (pH 8.0), 137mM NaCl, 10% glycerol, 1% Triton X-100, and 2 mM EDTA, and supplemented with protease and phosphatase inhibitors. Tissue lysates (300 μg of protein) were incubated in an orbital shaker for 1 hour at room temprature with protein A-agarose bead suspention (50 ul; sc-2001, Santa Cruz). Subsequently, supernatants were transferred to a fresh microtube and then incubated with p62 antibody (p0067, MilliporeSigma) and protein A-agarose bead suspention (50 ul) in an orbital shaker at 4°C overnight. After the overnight incubation, samples were centrifuged at 1000 rpm for 1 minute and the supernatant was discarded. The immunoprecipitated beads were then washed with sample lysis buffer 3 times and then washed in sample lysis buffer. Next, the immunoprecipitate was resuspended in 20 μl of sample lysis buffer, boiled for 3 minutes and loaded into an SDS-PAGE gel.

Real-time PCR

To assess Nrf2 mRNA expression in Nrf2 skmKO and p62 mTg/Nrf2 skmHET mice, total RNA was isolated from the plantaris muscle, heart, liver, kidney, and lung and reverse transcription was performed using the same protocol described for semiquantitative RT-PCR. Nrf2 and GAPDH mRNAs were quantified using the AriaMx Real Time PCR System (Agilent, Santa Clara, CA, USA) and SYBR Premix Ex taq II (Takara Bio, Shiga, Japan). All samples were run in duplicate. The following PCR primers were used: Nrf2: 5’-CGAGATATACGCAGGAGAGGTAAGA-3’ and 5’-GCTCGACAATGTTCTCCAGCTT-3’; and GAPDH: 5’-CCACATCGCTCAGACACCAT-3’ and 5’-ACCAAATCCGTTGACTCCGA-3’. Results were normalized by GAPDH mRNA and presented as fold change in relation to WT mice (28).

Assessment of autophagy flux

Colchicine (0.4 mg/kg in sterile dH_2O), a microtubule polymerization inhibitor used to block fusion of the lysosome to the autophagosome, or vehicle (proportional volume of sterile dH_2O) was administered intraperitoneally at 48 and 24 hours prior to tissue harvest as previously described (29–31)

Succinate dehydrogenase (SDH) staining

Tibialis anterior muscles were harvested and frozen in liquid nitrogen-cooled isopentane. Cross sections (8 μm) of the tibialis anterior muscle were stained a solution containing nitro blue tetrazolium (0.5 mg/mL) (FUJIFILM Wako Pure Chemical Co., Ltd., Osaka, Japan), sodium succinate (50 mM), and phosphate buffer (50 mM) for 30 min at 37 °C. Sections were rinsed with distilled water and mounted on slides with glycerol-based mounting medium. Images were acquired with a DS-Fi1 digital camera (Nikon) coupled to a BX43 optical microscope (Olympus) (32).

Statistical analysis

Data are presented as mean ± standard error (SE). Normality was tested using the Shapiro-Wilk test, and student's t-test, One-way ANOVA, Two-way ANOVA, and Chi-square test were used for statistical analyses as appropriate. The One-way and Two-way ANOVA were followed by a Tukey's multiple comparisons test, as applicable. If the distribution of the data was not normal, Mann-Whitney test, Kruskal-Wallis test, or Friedman's test were used instead of student's t-test, One-way ANOVA, and Two-way ANOVA. Values of $p<0.05$ were considered statistically significant and sample sizes are indicated in figure legends.

Results

Fast glycolytic muscles are more prone to oxidative stress and atrophy during cancer cachexia

Herein we used the well-established LLC implantation model to study cancer cachexia (Figure 1A) (23–25). LLC-induced cancer cachexia led to larger body and spleen weights primarily due to tumor growth (Figure 1B, C). Even though these were accompanied by atrophy of the glycolytic extensor digitorum longus (EDL), the mixed fiber-type tibialis anterior (TA) and gastrocnemius (GA), and the more oxidative soleus (SO) muscles (Figure 1D), more profound losses in mass occurred in the EDL, TA, and GA muscles in comparison to the SO muscle (−16.2%, −15.4%, and −13.5%, respectively, vs. −7.9%) (Figure 1E). Accordingly, grip strength was decreased by 42% with cancer cachexia (Figure 1F). Further examination of the TA muscle from LLC-implanted mice demonstrated no signs of necrosis, degeneration/regeneration, and infiltration of immune cells (Figure 1G). We were unable to obtain sufficient numbers of MyHCI fibers for a rigorous analysis in the TA muscle. However, MyHCIIa, MyHCIIb, and MyHCIId/x fibers displayed marked atrophy (Figure 1H–J). Under non-stressed conditions, oxidative muscles have larger basal expression of the Atrogin-1/MAFbx and MuRF1 proteins because these are likely required to sustain their increased protein turnover rates (33). Therefore, examining their induction by cancer cachexia across muscle types rather than their absolute expression can provide a better assessment of their contribution to the atrophy taking place. The expression of Atrogin-1/MAFbx and MuRF1 proteins were significantly higher during cancer cachexia in the glycolytic EDL muscle, while only MuRF1 was significantly higher in the more oxidative SO muscle (Figure 1K, L). Further, the magnitude of increase in Atrogin-1/MAFbx and MuRF1 proteins was disproportionate between these muscles, being ~170% in the EDL vs. ~70% for Atrogin-1/MAFbx and MuRF1 in the SO muscle (Figure 1M). Oxidative stress in skeletal muscle was assessed via MDA levels, a widely accepted marker of lipid peroxidation in this tissue (16, 34, 35). MDA assessment, however, requires a specific preparation of samples. Because the small EDL muscle was used for protein and mRNA analyses, we used another predominantly glycolytic, fast-twitch muscle (i.e., the white vastus lateralis) (16, 22, 36–38) as representative of overall oxidative stress in glycolytic muscles. Assessment of MDA-modified proteins demonstrated higher oxidative stress in the glycolytic white vastus lateralis (WV) muscle, but not in the SO muscle, during cancer cachexia (Figure 1N, O).

Altogether, these results extend previous findings indicating that glycolytic muscles are preferentially affected during LLC-induced cancer cachexia exhibiting oxidative stress, larger increases in the expression of E3 ubiquitin ligases and accentuated atrophy in comparison to the more oxidative SO muscle.

p62-Nrf2 pathway is less active in glycolytic versus oxidative muscles

Next, we interrogated the p62-Nrf2 pathway of antioxidant gene regulation in muscles with different fiber type composition (Figure 2A). Not surprisingly, the expression of several antioxidant proteins, such as MnSOD, EcSOD, NQO1, HO-1, and GSTM1 were significantly higher in the SO vs. the EDL muscle (Figure 2B, C). Nrf2 dissociation from Keap1 and its translocation to the nucleus are major signaling events in the p62-Nrf2 pathway regulating the expression of these antioxidant proteins. We then examined Nrf2, Keap1, and nuclear and cytoplasmic levels of Nrf2 proteins in these muscles. The purity of each fraction was confirmed by assessing Lamin B1, as a nuclear marker, and αβ-tubulin, as a cytoplasmic marker (Supplemental Figure S1A). Nrf2 and Keap1 were more abundant in the SO vs. the EDL muscle (~4-fold and ~1.5-fold, respectively) (Figure 2D, E). Nuclear levels of Nrf2 were ~1.6-fold higher, while cytoplasmic levels of Nrf2 were ~2.0-fold lower in the oxidative red portion vs. the glycolytic white portion of the GA muscle (Figure 2F, G). Next, we examined p62 levels in SO and EDL muscles. Both total and phosphorylated (Ser 351) p62 were significantly higher in the SO than in the EDL muscles (~1.6-fold and ~1.2-fold, respectively) (Figure 2H, I) and these were accompanied by higher interaction between p62 and Keap1 in the SO muscle (Figure 2J, Supplemental Figure S2A, B). Interestingly, the expression of total and phosphorylated (Ser351) p62 were significantly higher during cancer cachexia in the SO muscle, but not in the EDL muscle (Supplemental Figure S3A, B). Since increased NBR1, CK1, PKCδ, and TAK1 have been shown to either promote phosphorylation or directly phosphorylate p62 at Ser351 (39–42), we next measured the expression of these proteins and observed that all of those were significantly higher in the SO vs. the EDL muscles (Figure 2K, L).

Enhanced skeletal muscle-specific p62 expression activates Nrf2 and increases antioxidant protein expression

To determine whether p62 is sufficient to activate Nrf2 and increase levels of antioxidant proteins in skeletal muscle, we generated transgenic mice with muscle-specific overexpression of p62 under the control of the MCK promoter (p62 mTg). We obtained several lines of p62mTg mice and selected two lines showing either low [line L] or high [line H] overexpression of p62 to perform subsequent studies (Figure 3A, B, Supplemental Figure S4A, B). Total and phosphorylated (Ser351) p62 levels were significantly higher in glycolytic WV muscles of p62 mTg mice in both lines L (~3.2-fold and ~1.7-fold, respectively) and H (~41.8-fold and ~15.4-fold, respectively) vs. WT littermates (Figure 3C, D, Supplemental Figure S4C, D). Of note, the increases seen in total and phosphorylated p62 in muscles of line L are near physiological levels as those are similar to what was previously reported in muscles from mice undergoing exercise training (22). Nrf2 protein expression was not affected in both mouse lines, whereas Keap1 protein expression was increased only in line H of p62 mTg mice (Figure 3F, G, Supplemental Figure S4F, G). Importantly, p62 binding to Keap1 (Figure 3E, Supplemental Figure S4E), nuclear

Nrf2 protein (Figure 3H, I, Supplemental Figure S4H, I), and antioxidant proteins (i.e., CuZnSOD, MnSOD, EcSOD, and NQO1) (Figure 3J and K, Supplemental Figure S4J, K) were all higher in the glycolytic WV muscles of both p62 mTg lines when compared to WT mice. We expected some of these changes to also occur in oxidative muscles, and because all changes were more dramatic in the H line of p62 mTg mice, we then examined whether enhanced p62 levels affected Nrf2 regulation and antioxidant protein in the oxidative SO muscle of the L line of of p62 mTg mice. Again, total and phosphorylated (Ser351) p62 levels were significantly higher in p62 mTg mice than in WT mice (Supplemental Figure S7A, B). Total Nrf2 protein expression was also not affected by p62 overexpression in the SO, but Keap1 protein expression was significantly higher in p62 mTg mice vs. WT mice (Supplemental Figure S7C, D). Interestingly, a less prominent change in antioxidant proteins was observed in the SO muscle of p62 mTg mice, where only NQO1 protein expression was increased (Supplemental Figure S7E, F). Collectively, these observations indicate a broader impact of p62 overexpression on antioxidant proteins in glycolytic muscles. To gain further insight into whether these outcomes were directly dependent on p62, or resulting from other adaptations in glycolytic muscle, we then examined the expression of MyHC isoforms (MyHCI, IIa, and IIb), mitochondrial proteins (cytochrome oxidase IV and cytochrome c), and PGC-1α. These were unaltered in glycolytic muscles of lines L or H of p62 mTg when compared to their WT littermates, except cytochrome c and PGC-1α in line H (Supplemental Figure S5A, B, S6A, B). Staining for SDH activity also did not show significant differences between p62mTg in line L and WT mice (Supplemental Figure S5C). The enhanced expression of p62 could in theory have stimulated autophagy based on increased levels of p62 (Ser405) phosphorylation and elevated LC3II/I ratio observed in lines L and H of p62 mTg, and increased levels of Beclin1 in line H (Supplemental Figure S5D, E, S6D, F). We, therefore, assessed autophagy flux via colchicine administration, an inhibitor of microtubule-mediated delivery of autophagosomes to lysosomes, and observed a lower LC3-II accumulation and LC3-II/I ratio in line L and H of p62 mTg mice when compared to WT mice (Supplemental Figure S5F, G, S6E, F). These results indicate that p62 overexpression decreases autophagy flux. However, a potential p62-independent mechanism leading to Nrf2 activation when autophagy is impaired is very unlikely. Altogether these results indicate that the higher Nrf2 activation and antioxidant protein expression observed in glycolytic muscles of p62 mTg mice were likely a direct effect of enhanced p62 levels, rather than secondary outcomes altering key molecular pathways in skeletal muscles.

Near physiological increases in p62 expression do not affect muscle mass and function

To begin determining the functional impact of muscle p62 overexpression, we measured body weight, muscle weight, muscle fiber size, muscle endurance capacity (i.e., treadmill running test), and grip strength in line L and H of p62 mTg mice. Body weight, muscle weight (i.e., oxidative SO, mixed fiber-type TA and GA, and glycolytic EDL muscle), muscle endurance capacity, MyHCIIa, MyHCIIb, and MyHCIId/x muscle fiber size, and grip strength were not significantly different between line L of p62 mTg and WT mice (Figure 4A–D). The very small number of MyHCI fibers in the TA muscle hindered a rigorous comparison between genotypes. However, since the SO muscle weight was not different between these mice, very likely MyHCI fiber size was also not affected in line L of p62 mTg mice. Importantly, however, in line H of p62 mTg mice, body weight

was 4.4% lower than in WT mice (Supplemental Figure S8A). TA, GA, and EDL muscle weights were also significantly smaller in line H of p62 mTg mice than in WT mice (−7.5%, −9.6%, and −8.2%, respectively) (Supplemental Figure S8B). H&E staining in TA muscle demonstrated no signs of necrosis, degeneration/regeneration, and infiltration of immune cells in either the L or the H line of p62 mTg (Figure 4E, Supplemental Figure S8E). However, MyHCIIa, MyHCIIb, and MyHCIId/x fiber sizes were smaller in line H (Supplemental Figure S8F–H). As described for line L, we were unable to robustly assess the size of MyHCI fibers in the TA muscle but those were likely also not affected in line H of p62 mTg since because SO muscle weight was unaltered (Supplemental Figure S8B). Consistent with smaller MyHCII fiber sizes, running capacity was not significantly different, but grip strength was significantly lower in line H of p62 mTg mice than in WT mice (−13.0%) (Supplemental Figure S8C, D). Collectively, these results indicate that near physiological increases in muscle p62 do not negatively affect muscle morphology, size and function, whereas large p62 overexpression can be detrimental decreasing muscle mass and strength.

p62-mediated stimulation of antioxidant protein expression in muscle is partially dependent on Nrf2

To test the role of Nrf2 in the p62-mediated stimulation of antioxidant protein expression, we took advantage of p62 mTg mice with high p62 expression (H line) and generated mice with muscle-specific p62 overexpression and skeletal muscle-specific Nrf2 deficiency (p62 mTg/Nrf2 skmHET) (Figure 5A, Supplemental Figure S9A, B, and S10A). The rationale for using the H line was that determining changes in p62-Nrf2 signaling would be easier when p62 levels are substantially increased. As expected, p62 mRNA was increased substantially in the plantaris muscle of p62 mTg/Nrf2 skmHET mice when compared to $Nrf2^{f/+}$ mice (Figure 5B). p62 mRNA was also higher, but not as dramatically, in the heart of p62 mTg/Nrf2 skmHET mice in comparison to $Nrf2^{f/+}$ mice (Figure 5B). Nrf2 mRNA and protein levels were significantly lower only in skeletal muscle of Nrf2 skmHET and p62 mTg/Nrf2 skmHET mice in comparison to $Nrf2^{f/+}$ mice (Figure 5B, C). Total and phosphorylated (Ser351) p62 protein levels were not affected by Nrf2 deficiency (i.e., in p62 mTg/Nrf2 skmHET vs. p62 mTg/$Nrf2^{f/+}$ mice; Figure 5D, E). Several antioxidant proteins (i.e., CuZnSOD, MnSOD, EcSOD, NQO1, and GSTM1) were higher in muscles of p62 mTg/$Nrf2^{f/+}$ vs. $Nrf2^{f/+}$ mice. Muscle Nrf2 deficiency (i.e., in p62 mTg/Nrf2 skmHET) completed prevented the increase in EcSOD, blunted increases in CuZnSOD and NQO1 proteins but did not affect the increase in MnSOD when compared to p62 mTg/$Nrf2^{f/+}$ mice (Figure 5D, E). Even though these results support a strong role for Nrf2 activation in p62-mediated increases of EcSOD, CuZnSOD,and NQO1 expression in muscle, these also indicate that additional unknown mechanisms downstream of p62 stimulate the expression of CuZnSOD and NQO1. Of note, p62-mediated induction of MnSOD appears to be independent of Nrf2.

p62 overexpression alleviates glycolytic muscle atrophy in cancer cachexia

Lastly, we examined whether near physiological increases in p62, as seen in line L of p62 mTg, would provide protection against muscle atrophy in LLC-induced cancer cachexia (Figure 6A). Cancer cachexia increased body weight and spleen weight in both p62 mTg and WT mice (Figure 6B, C). However, overexpression of skeletal muscle p62 significantly

blunted the decreases in mass of the mixed-fiber TA and GA muscles and of the glycolytic EDL muscle during cancer cachexia (Figure 6D, E). A significant protection in the SO muscle of p62 mTg mice was not observed likely because the magnitude of cancer cachexia-induced atrophy in this muscle is small and, therefore, a larger number of animals would likely be required to precisely address this question. Cachexia-induced muscle weakness, as indicated by grip strength, was blunted in p62 mTg mice (i.e., −30% vs. −51% in WT mice) (Figure 6F). The mixed-fiber TA muscle of LLC-implanted mice demonstrated no signs of necrosis, degeneration/regeneration, and infiltration of immune cells in both p62mTg and WT mice (Figure 6G). MyHCIIa, MyHCIIb, and MyHCIId/x fiber size distribution was preserved in p62 mTg mice (Figure 6H, I). Minimum Feret's diameter of MyHCIIb and MyHCIId/x was also preserved in p62 mTg mice (Figure 6H, J). This observed protection of muscle mass and strength was accompanied by lower cancer cachexia-induced oxidative stress, as indicated by decreased MDA levels (Figure 6K, L). These results indicate that enhanced p62 expression in skeletal muscle is sufficient to increase antioxidant protein expression and suppress oxidative stress in glycolytic/fast twitch muscle fibers during LLC-induced cachexia, thereby preserving muscle mass and strength.

Discussion

Skeletal muscle atrophy resulting from cancer cachexia is associated with increased treatment-related toxicity (43) and decreased quality of life (44) and survival (45). Despite the multifaceted nature of cancer cachexia, oxidative stress has been shown to be a chief contributor to muscle wasting in that context (46). However, the mechanisms involved remain incompletely understood. The current study extends previous observations (3, 4) denoting that oxidative muscles (i.e., containing large proportions of MyHCI fibers) are more resistant to oxidative stress and atrophy during cancer cachexia than glycolytic muscles (i.e., composed primarily of MyHCIIa, MyHCIId/x, and MyHCIIb fibers). Although antioxidant protein expression is modulated by different mechanisms, in the present study we focused on p62, which is a protein involved in multiple cellular functions including signal transduction as well as degradation of proteins and organelles (47, 48). p62 function has been found to be modulated by multiple phosphorylation events. Phosphorylation of p62 at Ser403 (Ser405 in mice) enhances its adaptor role in ubiquitinated protein degradation, while phosphorylation at Ser349 (Ser 351 in mice) increases its affinity for Keap1 causing Nrf2 dissociation and nuclear translocation (13). Of note, in hepatocellular carcinoma cells, p62 is constitutively phosphorylated at Ser351 causing continuous activation of Nrf2 to prevent oxidative stress (14). Here, we observed that oxidative muscles have higher levels of p62 (total and Ser 351 phosphorylated) and p62 binding activity to Keap1 when compared to glycolytic muscles. These are accompanied by larger expression of proteins known to promote Ser 351 phosphorylation of p62 (i.e., NBR1, CK1, PKCδ, and TAK1) in oxidative muscles. These initial observations suggested for the first time that the enhanced antioxidant defense in oxidative vs. glycolytic muscles was at least partially due to a more active p62-Nrf2 pathway.

To address this question more directly, we first generated two muscle-specific lines with low and high levels of p62 overexpression (lines L and H, respectively). These were then used to determine if Nrf2 is required for p62-mediated modulation of antioxidant proteins and if

p62 could protect against cancer cachexia in muscle. We demonstrated with these p62 mTg mice that enhanced p62 in skeletal muscle leads to higher levels of phosphorylated p62, nuclear Nrf2 protein, and antioxidant protein expression. As expected, these outcomes were generally more prominent in line H vs. line L of p62 mTg.

As previously described and reiterated by our current data, Nrf2 levels and antioxidant protein expression are regulated in parallel with slow contractile proteins, mitochondria content, and PGC-1α expression (22, 49). However, these were unaltered in p62 mTg (both L and H lines) in comparison to WT littermates indicating that Nrf2 activation and higher antioxidant protein expression were direct outcomes of p62 overexpression in skeletal muscle.

Since p62 serves as an autophagy adaptor that accumulates when the process is deficient (50), we also examined this process in p62 mTg mice. Our results demonstrated that autophagy flux was actually lower in both L and H lines of p62 mTg mice when compared with WT mice. Interestingly, these observations indicate that a forced increase in p62 can also impair autophagy in muscle. The mechanisms involved remain to be determined, but because robust impairments in autophagy lead to muscle atrophy and weakness (50), the observed autophagy deficiency may have contributed to the smaller muscles seen in the H line of p62 mTg mice. In addition, p62 participates in the regulation of several pathways affecting not only antioxidant proteins and autophagy but also ubiquitin, inflammatory response, mTOR and ERK signaling (13). All of these might have been more prominently affected in the H line of p62 mTg impacting muscle homeostasis.

Next, to test the role of Nrf2 in p62-mediated regulation of antioxidant protein expression in muscle, we studied p62 mTg (line H) mice with skeletal muscle Nrf2 haplodeficiency (Nrf2 skmHET). Nrf2 deficiency did not alter total or phosphorylated levels of p62. However, Nrf2 was found to be required for p62-mediated induction of EcSOD, partially required for the induction of CuZnSOD,and NQO1, and dispensable for the induction of MnSOD. Future studies are still required to determine the p62-dependent, Nrf2-independent mechanisms of regulation of antioxidant protein expression in muscle.

To test the therapeutic potential of p62, we investigated whether enhanced p62 (near physiological levels) could limit muscle atrophy and weakness caused by cancer cachexia. After implanting LLC in line L of p62 mTg mice we observed that the losses of muscle strength, muscle weight, and muscle fiber size were all significantly decreased in comparison to WT mice. Importantly, although MDA levels were similar between p62 mTg and WT mice at baseline, which may be due to different rates of MDA turnover, MDA was also significantly diminished in parallel to higher expression of antioxidant proteins in p62 mTg during cancer cachexia. These results strongly indicate that near physiological increases in p62 (i.e., ~3-fold) can be protective against cancer cachexia by enhancing several muscle antioxidant proteins and decreasing oxidative stress in more glycolytic muscles.

Increased muscle contractile activity, as observed with regular exercise, prevents oxidative stress-induced muscle atrophy, at least partially, by improving the antioxidant defense

system (49, 51–53). We have previously reported that regular exercise increases antioxidant proteins, nuclear Nrf2 protein, and Nrf2 DNA-binding activity in association with increased p62 phosphorylation (Ser351) in mouse muscle (22) thereby demonstrating an effective strategy to stimulate the p62-Nrf2 pathway. However, future studies examining if the beneficial effects of exercise in cancer cachexia are dependent on the p62-Nrf2 pathway are still required.

In summary, the present study demonstrates that p62 is a potential target for therapy in cancer cachexia as its overexpression alleviates cancer-induced muscle wasting. Further, p62-mediated protection leads to increased expression of antioxidant proteins and a robust decrease in oxidative stress, which are at least partially dependent on Nrf2 activation in muscle.

Supplementary Material

Refer to Web version on PubMed Central for supplementary material.

Acknowledgments

The authors thank Dr. Steven J. Burden (New York University, New York, USA) and Dr. Jingbo Pi (China Medical University, Shenyang, China) for their generosity in providing Mlc1f-Cre mice and Nrf2 flox, respectively. The authors also thank Dr. Ichiro Miyoshi (Tohoku University, Sendai, Japan), Dr. Masayuki Yamamoto (Tohoku University), Dr. Takahumi Suzuki (Tohoku University), and Yasuo Kitajima (Hiroshima University, Hiroshima, Japan) for the arrangement of transfer of the mice. This study was supported by Grant-in-Aid for Scientific Research (B) (15H03080, 18H03153, 21H03326), Grant-in-Aid for Exploratory Research (20K21766), Suzuken Memorial Foundation, Toyoaki Scholarship Foundation, The Nakatomi Foundation, The Uehara Memorial Foundation, and Grant-in-Aid for Research in Nagoya City University (2321103) (to M.O.). This research was also supported by the National Institutes of Health R56AG063820 (to V.A.L.), Grant-in-Aid for JSPS Fellows (20J15551), Grant-in-Aid for Early-Career Scientists (22K17733), Suzuken Memorial Foundation, The Nakatomi Foundation, and The Uehara Memorial Foundation (to M.Y.).

Data Availability Statement

The data that support the findings of this study are available on request from the corresponding author.

Nonstandard Abbreviations

p62	sequestosome1/SQSTM1
Keap1	Kelch-like ECH-associated protein 1
Nrf2	Nuclear factor erythroid 2-related factor 2
ARE/EpRE	antioxidant/electrophile responsive element
NQO1	NAD(P)H-quinone oxidoreductase 1
HO-1	heme oxygenase 1
GSTM1	glutathione S-transferase M 1
CuZnSOD	cupper/zinc superoxide dismutase

MnSOD	manganese superoxide dismutase
EcSOD	extracellular superoxide dismutase
NBR1	BRCA1 gene 1
CK1	casein kinase 1
PKCδ	protein kinase C δ
TAK1	transforming growth factor-β activated kinase 1
LLC	Lewis Lung Carcinoma
MCK	muscle creatine kinase
mlc1f	myosin light chain 1 fast
mTg	muscle-specific overexpression
skmKO	muscle-specific knockout
skmHET	muscle-specific haplodeficiency
WT	wild-type
MyHC	myosin heavy chain
PGC-1α	peroxisome proliferator-activated receptor γ coactivator-1α
Atrogin-1/MAFbx	atrogin-1/muscle atrophy F-box
MuRF1	muscle RING finger 1
COX IV	cytochrome c oxidase subunit IV
LC3	microtubule-associated protein 1A/1B-light chain 3
Atg7	autophagy related 7
MDA	malondialdehyde
GAPDH	glyceraldehyde-3-phosphate dehydrogenase
SO	soleus
PL	plantaris
GA	gastrocnemius
TA	tibialis anterior muscles
EDL	extensor digitorum longus
WV	white vastus lateralis

References

1. Fearon K, Strasser F, Anker SD, Bosaeus I, Bruera E, Fainsinger RL, Jatoi A, Loprinzi C, MacDonald N, Mantovani G, Davis M, Muscaritoli M, Ottery F, Radbruch L, Ravasco P, Walsh D, Wilcock A, Kaasa S, and Baracos VE (2011) Definition and classification of cancer cachexia: an international consensus. The Lancet. Oncology 12, 489–495 [PubMed: 21296615]
2. Fearon KC, Glass DJ, and Guttridge DC (2012) Cancer cachexia: mediators, signaling, and metabolic pathways. Cell metabolism 16, 153–166 [PubMed: 22795476]
3. Brown JL, Lawrence MM, Ahn B, Kneis P, Piekarz KM, Qaisar R, Ranjit R, Bian J, Pharaoh G, Brown C, Peelor FF 3rd, Kinter MT, Miller BF, Richardson A, and Van Remmen H (2020) Cancer cachexia in a mouse model of oxidative stress. Journal of cachexia, sarcopenia and muscle 11, 1688–1704 [PubMed: 32918528]
4. Alves CRR, Eichelberger EJ, das Neves W, Ribeiro MAC, Bechara LRG, Voltarelli VA, de Almeida NR, Hagen L, Sharma A, Ferreira JCB, Swoboda KJ, Slupphaug G, and Brum PC (2021) Cancer-induced muscle atrophy is determined by intrinsic muscle oxidative capacity. Faseb j 35, e21714 [PubMed: 34118107]
5. Suzuki T, and Yamamoto M (2015) Molecular basis of the Keap1-Nrf2 system. Free Radic Biol Med 88, 93–100 [PubMed: 26117331]
6. Baird L, and Yamamoto M (2020) The Molecular Mechanisms Regulating the KEAP1-NRF2 Pathway. Mol Cell Biol 40
7. Cullinan SB, Gordan JD, Jin J, Harper JW, and Diehl JA (2004) The Keap1-BTB protein is an adaptor that bridges Nrf2 to a Cul3-based E3 ligase: oxidative stress sensing by a Cul3-Keap1 ligase. Mol Cell Biol 24, 8477–8486 [PubMed: 15367669]
8. Kobayashi A, Kang MI, Okawa H, Ohtsuji M, Zenke Y, Chiba T, Igarashi K, and Yamamoto M (2004) Oxidative stress sensor Keap1 functions as an adaptor for Cul3-based E3 ligase to regulate proteasomal degradation of Nrf2. Mol Cell Biol 24, 7130–7139 [PubMed: 15282312]
9. Kobayashi A, Ohta T, and Yamamoto M (2004) Unique function of the Nrf2-Keap1 pathway in the inducible expression of antioxidant and detoxifying enzymes. Methods Enzymol 378, 273–286 [PubMed: 15038975]
10. Kobayashi M, and Yamamoto M (2005) Molecular mechanisms activating the Nrf2-Keap1 pathway of antioxidant gene regulation. Antioxid Redox Signal 7, 385–394 [PubMed: 15706085]
11. Matzinger M, Fischhuber K, and Heiss EH (2018) Activation of Nrf2 signaling by natural products-can it alleviate diabetes? Biotechnology advances 36, 1738–1767 [PubMed: 29289692]
12. Onoki T, Izumi Y, Takahashi M, Murakami S, Matsumaru D, Ohta N, Wati SM, Hatanaka N, Katsuoka F, Okutsu M, Yabe Y, Hagiwara Y, Kanzaki M, Bamba T, Itoi E, and Motohashi H (2021) Skeletal muscle-specific Keap1 disruption modulates fatty acid utilization and enhances exercise capacity in female mice. Redox biology 43, 101966 [PubMed: 33857757]
13. Katsuragi Y, Ichimura Y, and Komatsu M (2015) p62/SQSTM1 functions as a signaling hub and an autophagy adaptor. FEBS J 282, 4672–4678 [PubMed: 26432171]
14. Komatsu M, Kurokawa H, Waguri S, Taguchi K, Kobayashi A, Ichimura Y, Sou YS, Ueno I, Sakamoto A, Tong KI, Kim M, Nishito Y, Iemura S, Natsume T, Ueno T, Kominami E, Motohashi H, Tanaka K, and Yamamoto M (2010) The selective autophagy substrate p62 activates the stress responsive transcription factor Nrf2 through inactivation of Keap1. Nature cell biology 12, 213–223 [PubMed: 20173742]
15. Ichimura Y, Waguri S, Sou YS, Kageyama S, Hasegawa J, Ishimura R, Saito T, Yang Y, Kouno T, Fukutomi T, Hoshii T, Hirao A, Takagi K, Mizushima T, Motohashi H, Lee MS, Yoshimori T, Tanaka K, Yamamoto M, and Komatsu M (2013) Phosphorylation of p62 activates the Keap1-Nrf2 pathway during selective autophagy. Molecular cell 51, 618–631 [PubMed: 24011591]
16. Okutsu M, Call JA, Lira VA, Zhang M, Donet JA, French BA, Martin KS, Peirce-Cottler SM, Rembold CM, Annex BH, and Yan Z (2014) Extracellular superoxide dismutase ameliorates skeletal muscle abnormalities, cachexia, and exercise intolerance in mice with congestive heart failure. Circ Heart Fail 7, 519–530 [PubMed: 24523418]
17. Call JA, Chain KH, Martin KS, Lira VA, Okutsu M, Zhang M, and Yan Z (2015) Enhanced skeletal muscle expression of extracellular superoxide dismutase mitigates streptozotocin-induced

diabetic cardiomyopathy by reducing oxidative stress and aberrant cell signaling. Circ Heart Fail 8, 188–197 [PubMed: 25504759]

18. Call JA, Donet J, Martin KS, Sharma AK, Chen X, Zhang J, Cai J, Galarreta CA, Okutsu M, Du Z, Lira VA, Zhang M, Mehrad B, Annex BH, Klibanov AL, Bowler RP, Laubach VE, Peirce SM, and Yan Z (2017) Muscle-derived extracellular superoxide dismutase inhibits endothelial activation and protects against multiple organ dysfunction syndrome in mice. Free Radic Biol Med 113, 212–223 [PubMed: 28982599]
19. Bothe GW, Haspel JA, Smith CL, Wiener HH, and Burden SJ (2000) Selective expression of Cre recombinase in skeletal muscle fibers. Genesis 26, 165–166 [PubMed: 10686620]
20. Xue P, Hou Y, Chen Y, Yang B, Fu J, Zheng H, Yarborough K, Woods CG, Liu D, Yamamoto M, Zhang Q, Andersen ME, and Pi J (2013) Adipose deficiency of Nrf2 in ob/ob mice results in severe metabolic syndrome. Diabetes 62, 845–854 [PubMed: 23238296]
21. Harada H, Warabi E, Matsuki T, Yanagawa T, Okada K, Uwayama J, Ikeda A, Nakaso K, Kirii K, Noguchi N, Bukawa H, Siow RC, Mann GE, Shoda J, Ishii T, and Sakurai T (2013) Deficiency of p62/Sequestosome 1 causes hyperphagia due to leptin resistance in the brain. The Journal of neuroscience : the official journal of the Society for Neuroscience 33, 14767–14777 [PubMed: 24027277]
22. Yamada M, Iwata M, Warabi E, Oishi H, Lira VA, and Okutsu M (2019) p62/SQSTM1 and Nrf2 are essential for exercise-mediated enhancement of antioxidant protein expression in oxidative muscle. FASEB J 33, 8022–8032 [PubMed: 30913396]
23. Busquets S, Toledo M, Orpí M, Massa D, Porta M, Capdevila E, Padilla N, Frailis V, López-Soriano FJ, Han HQ, and Argilés JM (2012) Myostatin blockage using actRIIB antagonism in mice bearing the Lewis lung carcinoma results in the improvement of muscle wasting and physical performance. Journal of cachexia, sarcopenia and muscle 3, 37–43 [PubMed: 22450815]
24. Ruas JL, White JP, Rao RR, Kleiner S, Brannan KT, Harrison BC, Greene NP, Wu J, Estall JL, Irving BA, Lanza IR, Rasbach KA, Okutsu M, Nair KS, Yan Z, Leinwand LA, and Spiegelman BM (2012) A PGC-1α isoform induced by resistance training regulates skeletal muscle hypertrophy. Cell 151, 1319–1331 [PubMed: 23217713]
25. Brown JL, Rosa-Caldwell ME, Lee DE, Blackwell TA, Brown LA, Perry RA, Haynie WS, Hardee JP, Carson JA, Wiggs MP, Washington TA, and Greene NP (2017) Mitochondrial degeneration precedes the development of muscle atrophy in progression of cancer cachexia in tumour-bearing mice. Journal of cachexia, sarcopenia and muscle 8, 926–938 [PubMed: 28845591]
26. Yamada M, Hokazono C, Tokizawa K, Marui S, Iwata M, Lira VA, Suzuki K, Miura S, Nagashima K, and Okutsu M (2019) Muscle-derived SDF-1alpha/CXCL12 modulates endothelial cell proliferation but not exercise training-induced angiogenesis. Am J Physiol Regul Integr Comp Physiol 317, R770–R779 [PubMed: 31577158]
27. Akimoto T, Ribar TJ, Williams RS, and Yan Z (2004) Skeletal muscle adaptation in response to voluntary running in Ca2+/calmodulin-dependent protein kinase IV-deficient mice. American journal of physiology. Cell physiology 287, C1311–1319 [PubMed: 15229108]
28. Okutsu M, Yamada M, Tokizawa K, Marui S, Suzuki K, Lira VA, and Nagashima K (2021) Regular exercise stimulates endothelium autophagy via IL-1 signaling in ApoE deficient mice. Faseb j 35, e21698 [PubMed: 34085350]
29. Ju JS, Varadhachary AS, Miller SE, and Weihl CC (2010) Quantitation of “autophagic flux” in mature skeletal muscle. Autophagy 6, 929–935 [PubMed: 20657169]
30. Milan G, Romanello V, Pescatore F, Armani A, Paik JH, Frasson L, Seydel A, Zhao J, Abraham R, Goldberg AL, Blaauw B, DePinho RA, and Sandri M (2015) Regulation of autophagy and the ubiquitin-proteasome system by the FoxO transcriptional network during muscle atrophy. Nature communications 6, 6670
31. Fuqua JD, Mere CP, Kronemberger A, Blomme J, Bae D, Turner KD, Harris MP, Scudese E, Edwards M, Ebert SM, de Sousa LGO, Bodine SC, Yang L, Adams CM, and Lira VA (2019) ULK2 is essential for degradation of ubiquitinated protein aggregates and homeostasis in skeletal muscle. Faseb j 33, 11735–11745 [PubMed: 31361156]
32. Nunomiya A, Shin J, Kitajima Y, Dan T, Miyata T, and Nagatomi R (2017) Activation of the hypoxia-inducible factor pathway induced by prolyl hydroxylase domain 2 deficiency enhances

the effect of running training in mice. Acta physiologica (Oxford, England) 220, 99–112 [PubMed: 27393382]

33. Goodman CA, Mabrey DM, Frey JW, Miu MH, Schmidt EK, Pierre P, and Hornberger TA (2011) Novel insights into the regulation of skeletal muscle protein synthesis as revealed by a new nonradioactive in vivo technique. Faseb j 25, 1028–1039 [PubMed: 21148113]
34. Kaczor JJ, Hall JE, Payne E, and Tarnopolsky MA (2007) Low intensity training decreases markers of oxidative stress in skeletal muscle of mdx mice. Free Radic Biol Med 43, 145–154 [PubMed: 17561103]
35. Ulla A, Osaki K, Rahman MM, Nakao R, Uchida T, Maru I, Mawatari K, Fukawa T, Kanayama HO, Sakakibara I, Hirasaka K, and Nikawa T (2022) Morin improves dexamethasone-induced muscle atrophy by modulating atrophy-related genes and oxidative stress in female mice. Bioscience, biotechnology, and biochemistry 86, 1448–1458 [PubMed: 35977398]
36. Lira VA, Okutsu M, Zhang M, Greene NP, Laker RC, Breen DS, Hoehn KL, and Yan Z (2013) Autophagy is required for exercise training-induced skeletal muscle adaptation and improvement of physical performance. FASEB J 27, 4184–4193 [PubMed: 23825228]
37. Carlson CJ, Booth FW, and Gordon SE (1999) Skeletal muscle myostatin mRNA expression is fiber-type specific and increases during hindlimb unloading. The American journal of physiology 277, R601–606 [PubMed: 10444569]
38. Castorena CM, Mackrell JG, Bogan JS, Kanzaki M, and Cartee GD (2011) Clustering of GLUT4, TUG, and RUVBL2 protein levels correlate with myosin heavy chain isoform pattern in skeletal muscles, but AS160 and TBC1D1 levels do not. Journal of applied physiology (Bethesda, Md. : 1985) 111, 1106–1117 [PubMed: 21799128]
39. Sánchez-Martín P, Sou YS, Kageyama S, Koike M, Waguri S, and Komatsu M (2020) NBR1-mediated p62-liquid droplets enhance the Keap1-Nrf2 system. EMBO reports 21, e48902 [PubMed: 31916398]
40. Sanz L, Diaz-Meco MT, Nakano H, and Moscat J (2000) The atypical PKC-interacting protein p62 channels NF-kappaB activation by the IL-1-TRAF6 pathway. The EMBO journal 19, 1576–1586 [PubMed: 10747026]
41. Sánchez-Martín P, Saito T, and Komatsu M (2019) p62/SQSTM1: 'Jack of all trades' in health and cancer. Febs j 286, 8–23 [PubMed: 30499183]
42. Kehl SR, Soos BA, Saha B, Choi SW, Herren AW, Johansen T, and Mandell MA (2019) TAK1 converts Sequestosome 1/p62 from an autophagy receptor to a signaling platform. EMBO reports 20, e46238 [PubMed: 31347268]
43. Blauwhoff-Buskermolen S, Versteeg KS, de van der Schueren MA, den Braver NR, Berkhof J, Langius JA, and Verheul HM (2016) Loss of Muscle Mass During Chemotherapy Is Predictive for Poor Survival of Patients With Metastatic Colorectal Cancer. Journal of clinical oncology : official journal of the American Society of Clinical Oncology 34, 1339–1344 [PubMed: 26903572]
44. Strasser F (2008) Diagnostic criteria of cachexia and their assessment: decreased muscle strength and fatigue. Current opinion in clinical nutrition and metabolic care 11, 417–421 [PubMed: 18542001]
45. Bachmann J, Heiligensetzer M, Krakowski-Roosen H, Büchler MW, Friess H, and Martignoni ME (2008) Cachexia worsens prognosis in patients with resectable pancreatic cancer. Journal of gastrointestinal surgery : official journal of the Society for Surgery of the Alimentary Tract 12, 1193–1201 [PubMed: 18347879]
46. Ábrigo J, Elorza AA, Riedel CA, Vilos C, Simon F, Cabrera D, Estrada L, and Cabello-Verrugio C (2018) Role of Oxidative Stress as Key Regulator of Muscle Wasting during Cachexia. Oxidative medicine and cellular longevity 2018, 2063179 [PubMed: 29785242]
47. Johansen T, and Lamark T (2011) Selective autophagy mediated by autophagic adapter proteins. Autophagy 7, 279–296 [PubMed: 21189453]
48. Nezis IP, and Stenmark H (2012) p62 at the interface of autophagy, oxidative stress signaling, and cancer. Antioxid Redox Signal 17, 786–793 [PubMed: 22074114]
49. Yan Z, Okutsu M, Akhtar YN, and Lira VA (2011) Regulation of exercise-induced fiber type transformation, mitochondrial biogenesis, and angiogenesis in skeletal muscle. Journal of applied physiology (Bethesda, Md. : 1985) 110, 264–274 [PubMed: 21030673]

50. Masiero E, Agatea L, Mammucari C, Blaauw B, Loro E, Komatsu M, Metzger D, Reggiani C, Schiaffino S, and Sandri M (2009) Autophagy is required to maintain muscle mass. Cell metabolism 10, 507–515 [PubMed: 19945408]

51. Powers SK, Radak Z, and Ji LL (2016) Exercise-induced oxidative stress: past, present and future. The Journal of physiology 594, 5081–5092 [PubMed: 26893258]

52. Yan Z, and Spaulding HR (2020) Extracellular superoxide dismutase, a molecular transducer of health benefits of exercise. Redox biology 32, 101508 [PubMed: 32220789]

53. Powers SK, Goldstein E, Schrager M, and Ji LL (2022) Exercise Training and Skeletal Muscle Antioxidant Enzymes: An Update. Antioxidants (Basel, Switzerland) 12

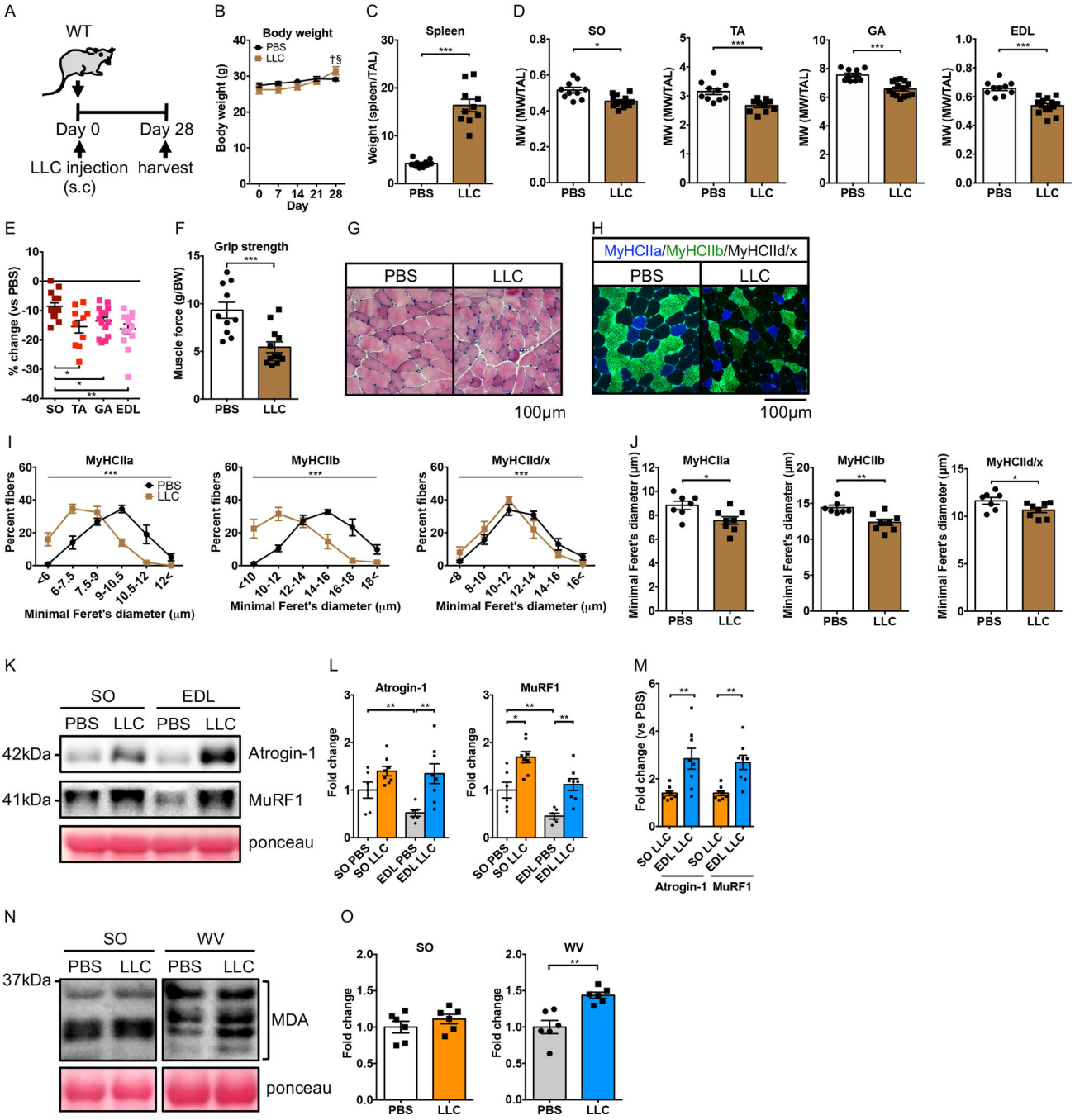

Figure 1.

Cancer cachexia causes larger atrophy and oxidative stress in glycolytic vs. oxidative muscles. A) Study design. B) Change of body weight in Lewis lung carcinoma (LLC) and PBS injected mice. C) Spleen weight in LLC and PBS injected mice. D) Oxidative soleus (SO), mixed fiber type of tibialis anterior (TA) and gastrocnemius (GA), and glycolytic extensor digitorum longus muscle (EDL) weight (normalized by tibia length) in LLC and PBS injected mice. E) Percent change of SO, TA, GA, and EDL muscle weight in LLC and PBS injected mice. F) Grip strength in LLC and PBS injected mice.

G) Hematoxylin and Eosin staining of TA muscle cross-sections stained in LLC and PBS injected mice. H) Immunofluorescence images of TA muscle cross-sections stained with antibodies for MyHCIIa (blue) and MyHCIIb (green) in LLC and PBS injected mice. Non-stained fibers were analyzed as MyHCIId/x (black). I) Histograms of MyHCIIa, MyHCIIb, and MyHCIId/x fiber size distribution in LLC and PBS injected mice according to cross-sectional area (n=7–8/group). J) Average minimal Feret's diameter of MyHCIIa, MyHCIIb, and MyHCIId/x fiber in LLC and PBS injected mice (n=7–8/group). K) Representative immunoblot images of Atrogin-1 and MuRF1 expression in SO and EDL muscle of LLC and PBS injected mice. L) Quantification of Atrogin-1 and MuRF1 expression in SO and EDL muscles of LLC and PBS injected mice (n=6–8/group). M) Comparison of Atrogin-1 and MuRF1 expression in SO and EDL muscle of LLC and PBS injected mice (n=8/group). N) Representative immunoblot images of MDA expression in SO and glycolytic white vastus lateralis (WV) muscle of LLC and PBS injected mice. O) Quantification of MDA expression in SO and WV muscle of LLC and PBS injected mice (n=6/group). Protein expression comparisons were performed after normalization to ponceau. Results are represented as means ± SE (n=10–14/group, unless specified otherwise). Scale bar=100 μm. Data was analyzed with unpaired t-test (C, D, F, J, M and O), One-way ANOVA followed by Tukey's multiple comparisons test (E), Two-way ANOVA followed by Tukey's multiple comparisons test (B and L), and Chi-square test (I). $*P<0.05$, $**P<0.01$, $***P<0.001$; †$P<0.05$ in comparison to other groups of the day; §$P<0.05$ in comparison to Day 0.

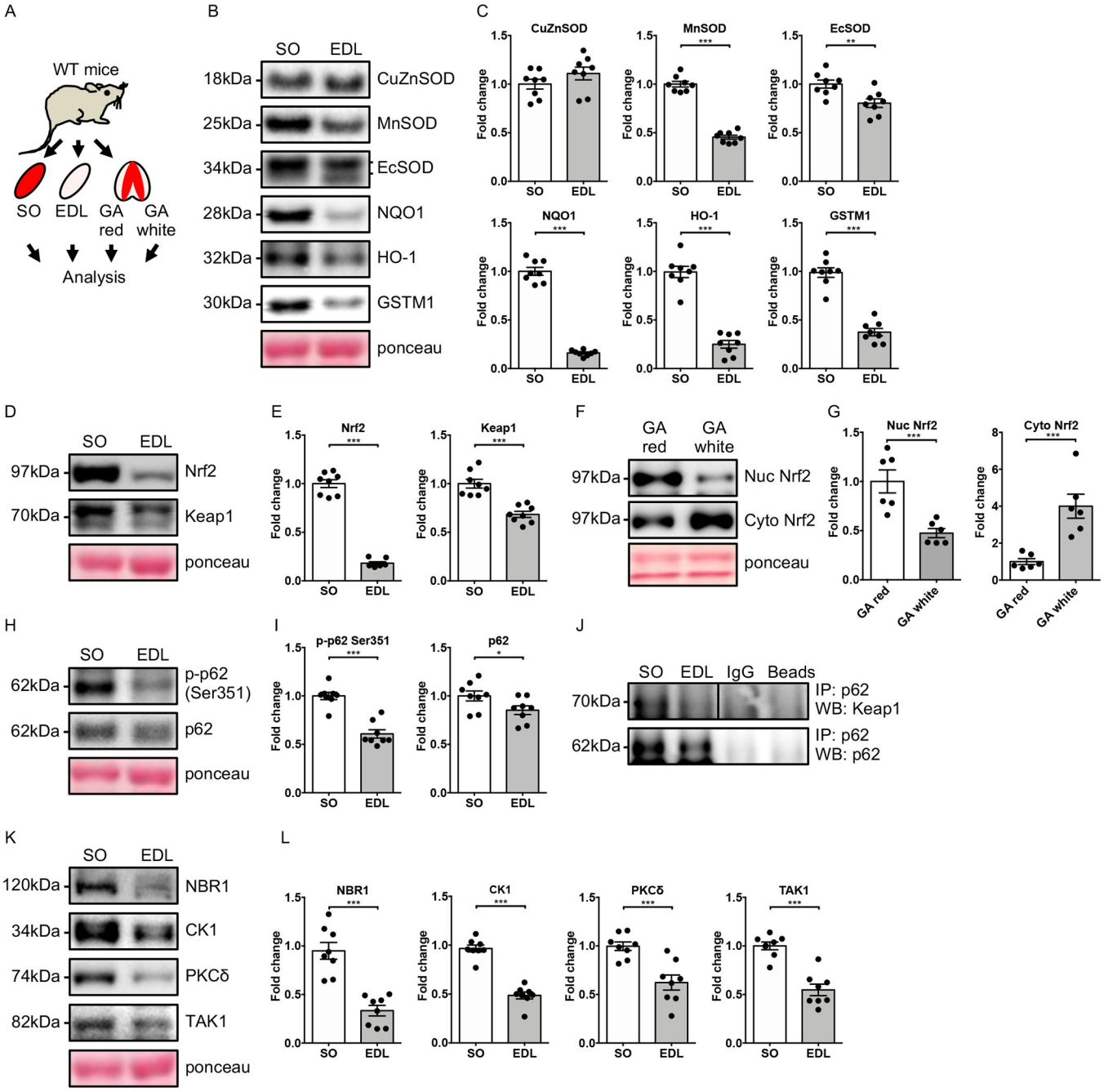

Figure 2.

Glycolytic muscles have lower Nrf2 activity than oxidative muscles in associated with lower p62 phosphorylation-inducible protein expression. A) Study design. B) Representative immunoblot images of antioxidant protein expression in oxidative soleus (SO) and glycolytic extensor digitorum longus muscle (EDL) muscle. C) Quantification of antioxidant proteins expression in SO and EDL muscles. D) Representative immunoblot images of Keap1 and Nrf2 protein expression in SO and EDL muscles. E) Quantification of Keap1 and Nrf2 proteins expression in SO and EDL muscles. F) Representative immunoblot images of nuclear and cytoplasmic Nrf2 protein (Nuc Nrf2 and Cyto Nrf2, respectively) in oxidative

muscle fiber abundant red portion of gastrocnemius (GA red) and glycolytic muscle fiber abundant white portion of gastrocnemius (GA white) muscles. G) Quantification of nuclear and cytoplasmic Nrf2 proteins in GA red and GA white muscles (n=6/group). H) Representative immunoblot images of phosphorylated p62 at Ser351 (p-p62 Ser351) and p62 protein expression in SO and EDL muscle. I) Quantification of p-p62 Ser351 and p62 proteins expression in SO and EDL muscles. J) Representative immunoblot images of co-immunoprecipitation analysis in the tibialis anterior muscle for Keap1 interaction with p62. Normal rabbit IgG and agarose beads alone were used as control. More than three independent experiments were conducted. K) Representative immunoblot images of NBR1, CK1, PKCδ, and TAK1 protein expression in SO and EDL muscle. L) Quantification of NBR1, CK1, PKCδ, and TAK1 proteins expression in SO and EDL muscle. Protein expression comparisons were performed after normalization to ponceau. Results are represented as means ± SE (n=8/group, unless specified otherwise). Data was analyzed with unpaired t-tests. *P<0.05, **P<0.01, ***P<0.001.

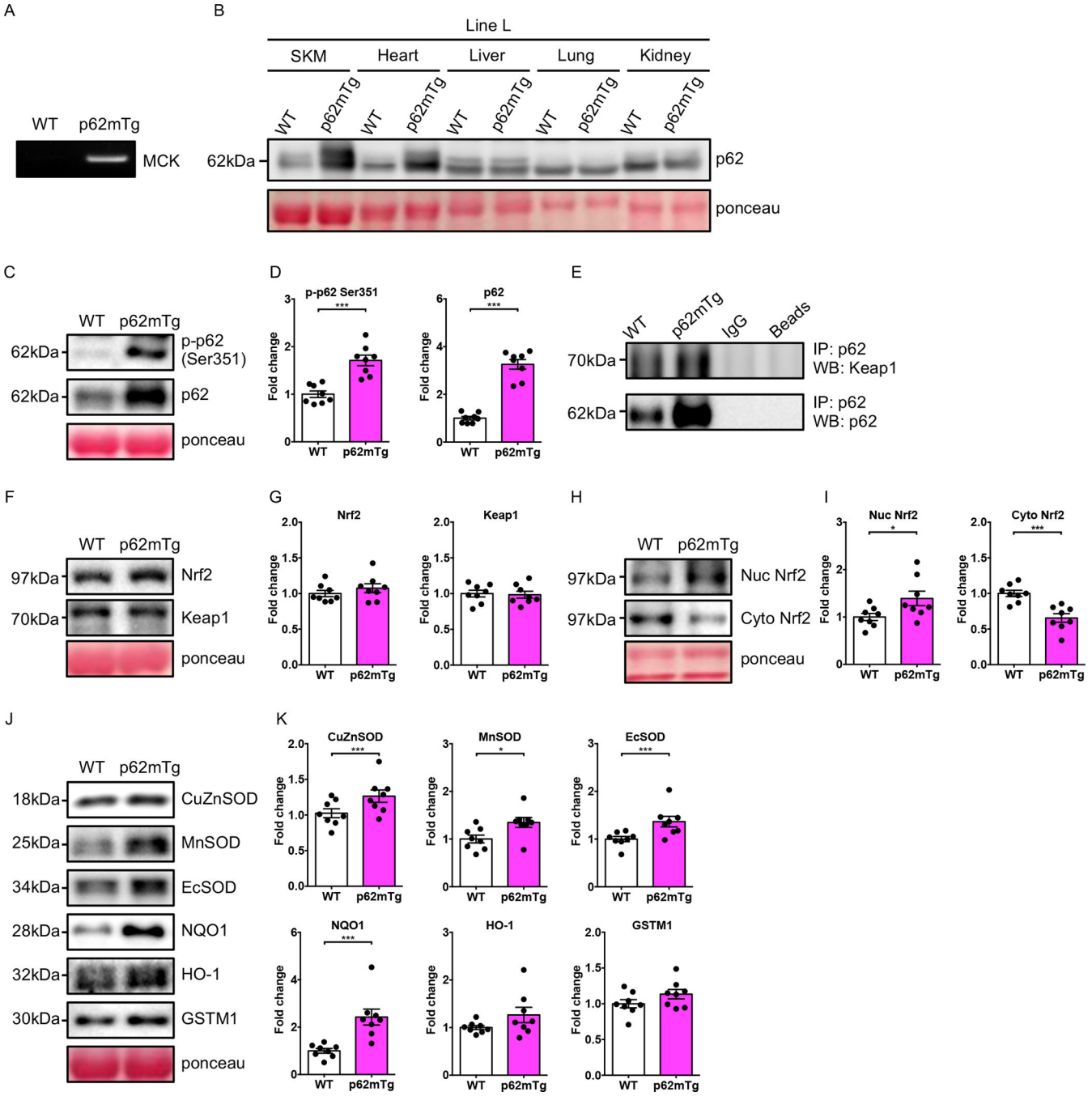

Figure 3.

Increased p62 expression induces Nrf2 activation and enhances antioxidant protein expression in skeletal muscle. A) PCR images of genotyping. B) Representative immunoblot denoting p62 protein expression of p62 mTg in line L and wild-type littermate (WT) mice in plantaris muscle (SKM), heart, liver, lung, and kidney. C) Representative immunoblot images of phosphorylated p62 at Ser351 (p-p62 Ser351) and p62 protein expression in glycolytic white vastus lateralis (WV) muscle of p62 mTg and WT mice. D) Quantification of p-p62 Ser351 and p62 proteins expression in WV muscle of p62 mTg and WT mice.

E) Representative immunoblot images of co-immunoprecipitation analysis in the tibialis anterior muscle for Keap1 interaction with p62. Normal rabbit IgG and agarose beads alone were used as control. More than three independent experiments were conducted. F) Representative immunoblot images of Keap1 and Nrf2 protein expression in WV muscle of p62 mTg and WT mice. G) Quantification of Keap1 and Nrf2 proteins expression in WV muscle of p62 mTg and WT mice. H) Representative immunoblot images of nuclear and cytoplasmic Nrf2 protein (Nuc Nrf2 and Cyto Nrf2, respectively) in white portion of gastrocnemius (GA white) muscle of p62 mTg and WT mice. I) Quantification of nuclear and cytoplasmic Nrf2 proteins in GA white muscle of p62 mTg and WT mice. J) Representative immunoblot images of antioxidant proteins expression in WV muscle of p62 mTg and WT mice. K) Representative immunoblot images of antioxidant proteins expression in WV muscle of p62 mTg and WT mice. Protein expression comparisons were performed after normalization to ponceau. Results are represented as means ± SE (n=8/group, unless specified otherwise). Data was analyzed with Mann-Whitney test for NQO1 (K) and Nuc Nrf2 (I), and unpaired t-tests for all other variables. *$P<0.05$, ***$P<0.001$.

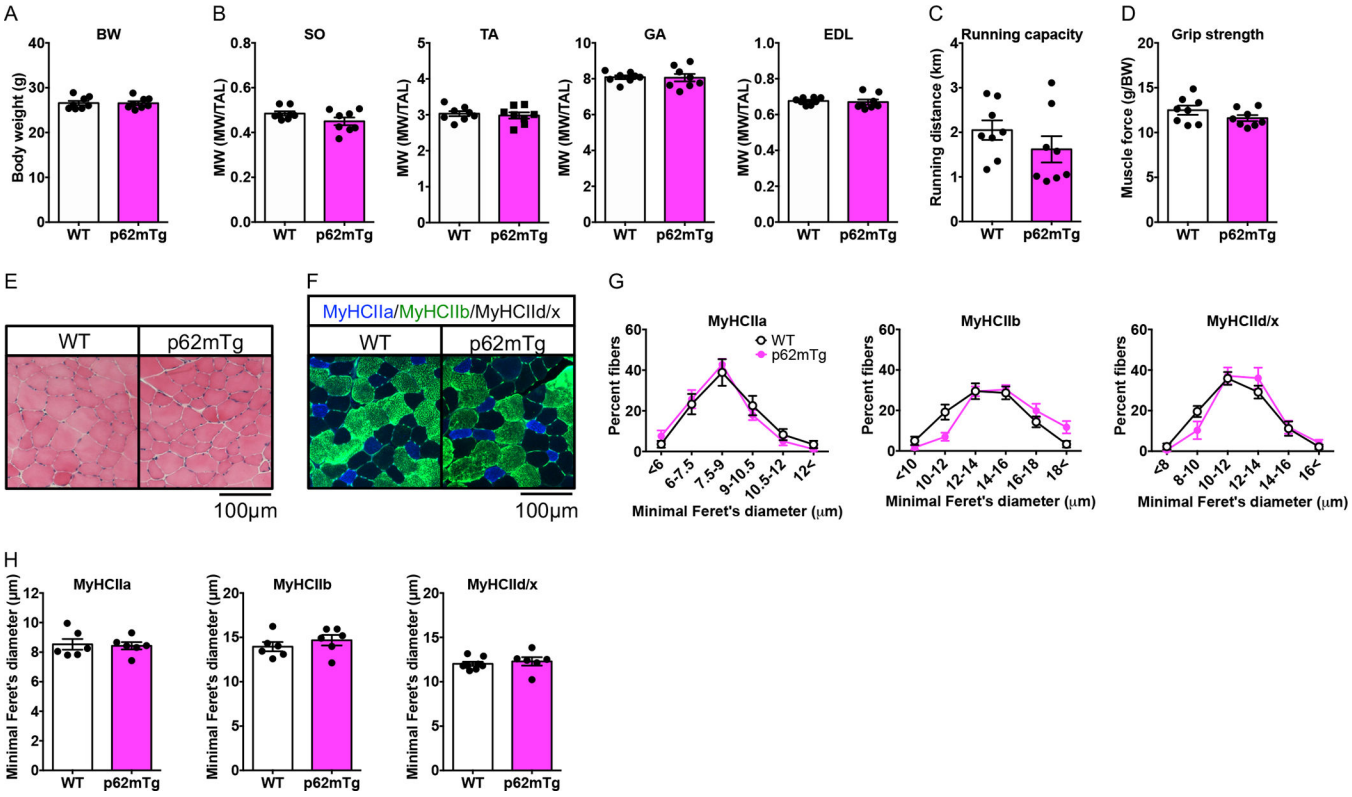

Figure 4.

Enhanced muscle-specific p62 expression at physiological level does not affect muscle mass and function. A) Body weight in line L of muscle-specific p62 overexpression (p62 mTg) and wild-type littermate (WT) mice. B) Oxidative soleus (SO), mixed fiber type of tibialis anterior (TA) and gastrocnemius (GA), and glycolytic extensor digitorum longus muscle (EDL) weight (normalized by tibia length) in line L of p62mTg and WT mice. C) Running capacity in line L of p62 mTg and WT mice. D) Grip strength in line L of p62 mTg and WT mice. E) Hematoxylin and Eosin staining of TA muscle cross-sections stained in line L of p62 mTg and WT mice. F) Immunofluorescence images of TA muscle cross-sections stained with antibodies for MyHCIIa (blue) and MyHCIIb (green) in line L of p62 mTg and WT mice. Non-stained fibers were analyzed as MyHCIId/x (black). G) Histograms of MyHCIIa, MyHCIIb, and MyHCIId/x fiber size distribution in line L of p62 mTg and WT mice according to cross-sectional area (n=6/group). H) Average minimal Feret's diameter of MyHCIIa, MyHCIIb, and MyHCIId/x fiber in line L of p62 mTg and WT mice (n=6/group). Results are represented as means ± SE (n=7–8/group, unless specified otherwise). Data was analyzed using unpaired t-test.

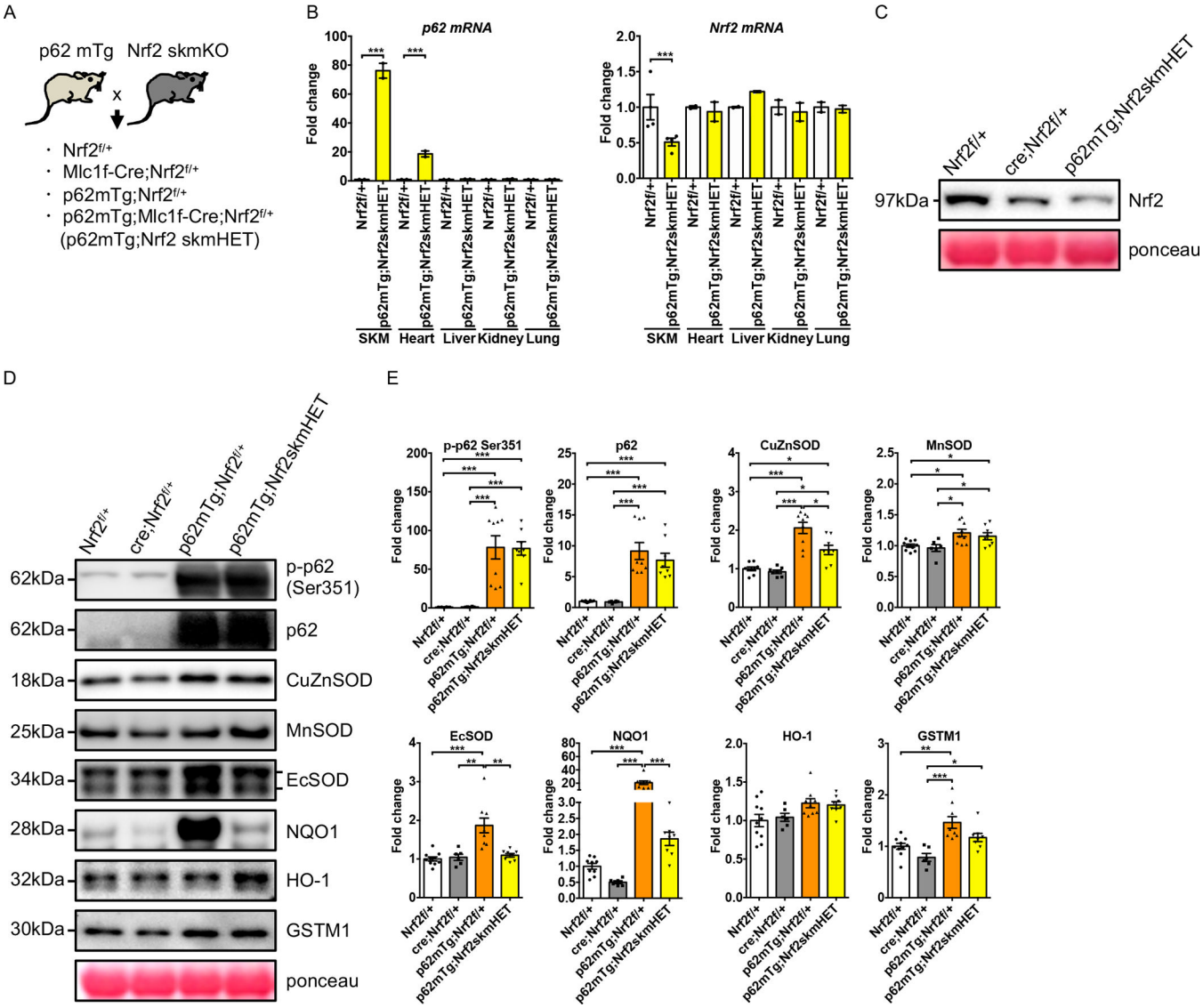

Figure 5.

Antioxidant protein expression of mice with muscle-specific p62 overexpressed muscle-specific Nrf2 haplodefficiency mice. A) Generation of the muscle-specific p62 overexpressed muscle-specific Nrf2 haplodefficiency mice (p62 mTg; Nrf2 skmHET). Mlc1f-Cre/Nrf2$^{f/f}$ (muscle-specific Nrf2 KO mice; Nrf2 skmKO) were mated to produce p62 mTg in line H mice, and then obtained Nrf2$^{f/+}$, Cre; Nrf2$^{f/+}$, p62mTg; Nrf2$^{f/+}$, and p62mTg; Nrf2 skmHET. B) p62 and Nrf2 mRNA expression in Nrf2$^{f/+}$ and p62mTg; Nrf2 skmHET mice in plantaris muscle (SKM), heart, liver, kidney, and lung (n=2–4/group). C) Representative immunoblot images of Nrf2 protein expression in isolated EDL muscle fibers of Nrf2$^{f/-}$ and p62mTg; Nrf2 skmHET mice.

D) Representative immunoblot images of phosphorylated p62 at Ser351(p-p62 Ser351), p62, CuZnSOD, MnSOD, EcSOD, NQO1, HO-1, and GSTM1 protein expression in WV muscle of p62mTg; Nrf2 skmHET and WT mice. E) Quantification of p-p62 Ser351, p62, CuZnSOD, MnSOD, EcSOD, NQO1, HO-1, and GSTM1 protein expression in WV

muscle of p62mTg; Nrf2 skmHET and WT mice. Protein expression comparisons were performed after normalization to ponceau. Results are represented as means ± SE (n=6–10/group, unless specified otherwise). Data was analyzed using unpaired t-test (B) and One-way ANOVA followed by Tukey's multiple comparisons test (E). *P<0.05, **P<0.01, ***P<0.001.

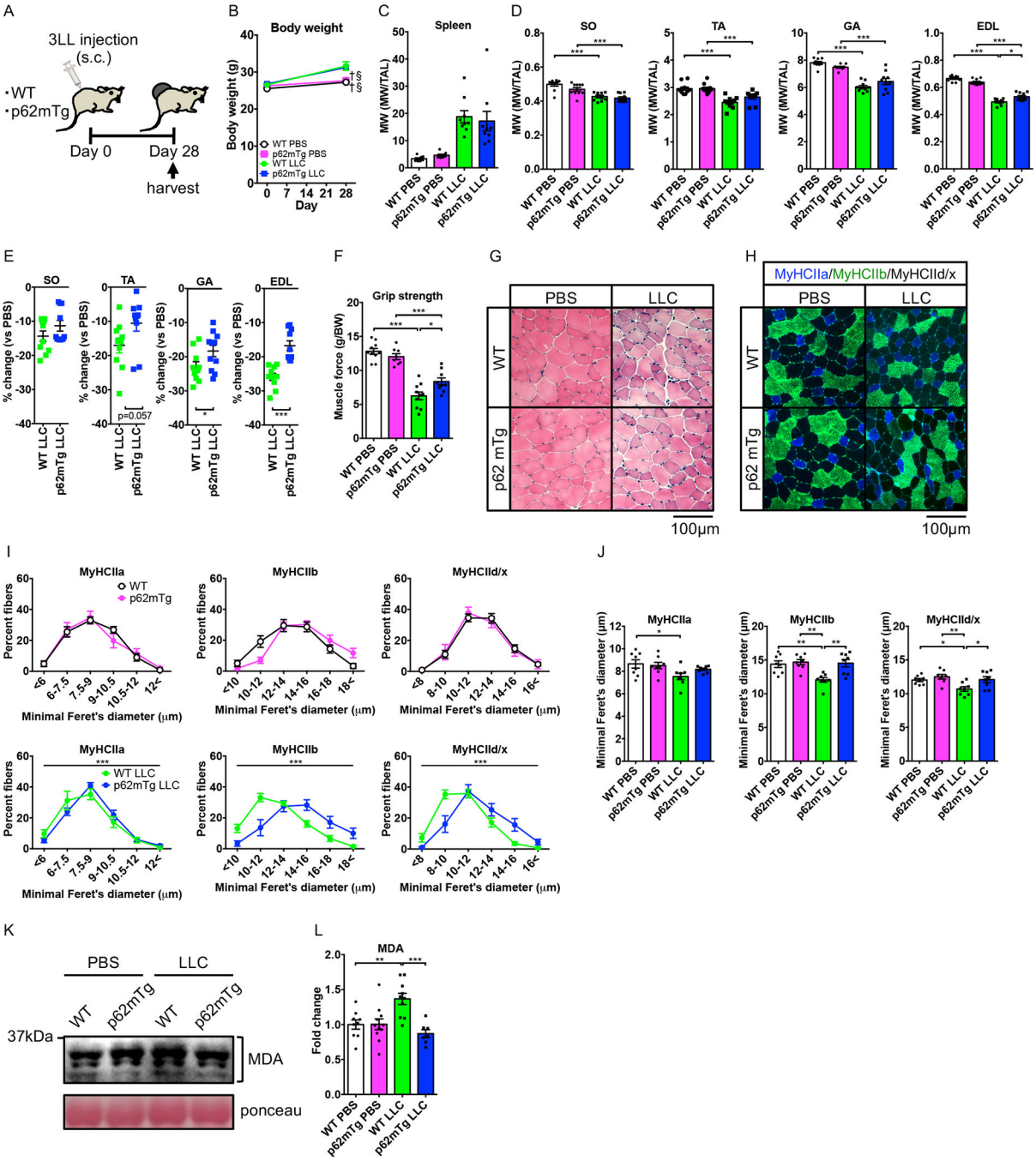

Figure 6.

p62 overexpression protects glycolytic muscles against cancer cachexia. A) Study design. B) Change of body weight in line L of p62 mTg and wild-type littermate (WT) mice injected with LLC cells or PBS. C) Spleen weight in line L of p62 mTg and WT mice injected with LLC cells or PBS (n=8–9/group). D) Oxidative soleus (SO), mixed fiber type of tibialis anterior (TA) and gastrocnemius (GA), and glycolytic extensor digitorum longus muscle (EDL) weight (normalized to tibia length) in line L of p62 mTg and WT mice injected with LLC cells or PBS. E) Percent change of SO, TA, GA, and EDL muscle weight in line L of

p62 mTg and WT mice injected with LLC cells or PBS. F) Grip strength in line L of p62 mTg and WT mice injected with LLC cells or PBS. G) Hematoxylin and Eosin staining of TA muscle cross-sections stained in line L of p62 mTg and WT mice injected with LLC cells or PBS. H) Immunofluorescence images of TA muscle cross-sections stained with antibodies for MyHCIIa (blue) and MyHCIIb (green) in line L of p62 mTg and WT mice injected with LLC cells or PBS. Non-stained fibers were analyzed as MyHCIId/x (black). I) Histograms of MyHCIIa, MyHCIIb, and MyHCIId/x fiber size distribution in line L of p62 mTg and WT mice injected with LLC cells or PBS according to cross-sectional area (n=8/group). J) Average minimal Feret's diameter of MyHCIIa, MyHCIIb, and MyHCIId/x fiber in line L of p62 mTg and WT mice injected with LLC cells or PBS (n=8/group). K) Representative immunoblot images of MDA expression in the glycolytic white vastus lateralis (WV) muscle of p62 mTg in line L and WT mice injected with LLC cells or PBS. L) Quantification of MDA expression in WV muscle of p62 mTg in line L and WT mice injected with LLC cells or PBS (n=7–11/group). Protein expression comparisons were performed after normalization to ponceau. Results are represented as means ± SE (n=10/group, unless specified otherwise). Data was analyzed using unpaired t-test (E), Two-way ANOVA followed by Tukey's multiple comparisons test (B, D, F, J, and L), Friedman's test (C), and Chi-square test (I). *P<0.05, **P<0.01, ***P<0.001; †P<0.05 in comparison to each control of day 28; §P<0.05 in comparison to each control of day 0.